

Tropical cyclone response to anthropogenic warming as simulated by a mesoscale-resolving global coupled earth system model

Authors: Jung-Eun Chu^{1,2}, Sun-Seon Lee^{1,2*}, Axel Timmermann^{1,2*}, Christian Wengel^{1,2}, Malte F. Stuecker³, Ryohei Yamaguchi^{1,2}

Author Affiliation:

¹Center for Climate Physics, Institute for Basic Science (IBS), Busan, South Korea, 46241.

²Pusan National University, Busan, South Korea, 46241.

³Department of Oceanography and International Pacific Research Center, University of Hawai'i at Mānoa, Honolulu, HI, USA.

***Corresponding Authors:**

Name: Sun-Seon Lee; Address: Center for Climate Physics, Institute for Basic Science (IBS), Pusan National University, Busan, South Korea, 46241; Phone: +82-51-510-7691; Email: sunseonlee@pusan.ac.kr

Axel Timmermann; Address: Center for Climate Physics, Institute for Basic Science (IBS), Pusan National University, Busan, South Korea, 46241; Phone: +82-51-510-2890; Email: axel@ibsclimate.org

Abstract

Tropical cyclones (TCs) are extreme storm systems that form over warm tropical oceans. Along their track TCs can mix up cold water which can further impact their development. Due to the adoption of lower ocean model resolutions, previous modeling studies on the TC response to greenhouse warming underestimate such oceanic feedbacks. To address the robustness of TC projections in the presence of mesoscale air-sea interactions, we conduct century-long present-day, CO₂ doubling and quadrupling experiments using the Community-Earth-System-Model 1.2.2 with ~25 km atmosphere and ~10 km ocean resolution. In these experiments an overall projected weakening of the rising branch of the Hadley Cells suppresses TC formation in the main genesis regions which weakens the TC-generated ocean cooling. Consistent with lower-resolution coupled modeling studies we find a reduction in global TC frequencies, a poleward shift of fast-moving extratropical TCs and an upsurge in precipitation rates and the intensity of landfalling events.

Keywords: tropical cyclones, extreme event, climate change, weather and climate, hurricanes, typhoons, ultra-high-resolution simulation, air-sea interaction

Tropical cyclones (TCs) are the most fatal and costliest weather disaster on our planet. It is therefore of utmost importance to understand how their tracks, intensity and associated rainfall patterns will change in response to greenhouse warming. A recent study(1) reveals consistent patterns in observed changes in TC occurrence and those simulated by climate models, leading to the conclusion that greenhouse warming may have already altered the statistics of TCs beyond the level of natural variability. However, there still remain major uncertainties in model-based projections of TCs, in part due to the effects of horizontal resolution(2, 3), atmosphere-ocean coupling(4, 5), the choice of physical parameterizations(6) and discretization of the underlying physical equations(7).

To determine the sensitivity of TC statistics and dynamics to radiative perturbations, three main dynamical modeling approaches have been adopted:

- i) In “pseudo global warming experiments”, Sea Surface Temperature (SST) boundary conditions for a high-resolution atmosphere general circulation model are obtained by adding SST responses from coarse resolution coupled earth system model projections onto the observed SST climatology(8-13). A key advantage of this method is that realistic observed SST conditions can be used for the control simulation. However, this approach ignores possible two-way interactions between atmosphere and ocean.
- ii) In fully coupled global earth system model simulations, either the atmosphere, ocean or both are run at horizontal resolutions which are suitable for representing mesoscale features(3, 14, 15). Even though this approach is computationally more intensive, it captures the interaction between TCs and the ocean more realistically. One disadvantage is that the coupled model SST climatology may still differ considerably in some regions from the observations. Such biases can influence the representation of TCs.

- iii) In regional atmosphere or coupled model experiments, coarse resolution model simulations are used as lateral boundary conditions(2). One of the key disadvantages is that depending on the domain size, the dynamics inside the region of interest is controlled by a mixture of prescribed horizontal boundary conditions, external forcing and internal dynamics. Oftentimes, the relative role of these factors is difficult to disentangle.

So far, the majority of studies on future changes in global TC statistics rely on the pseudo-global warming set-up(8-13) or on coupled models with relatively coarse resolution ocean models(3, 14) which use ~100 km horizontal resolution. Their main conclusions can be summarized as follows: global warming is likely to increase the TC intensity (frequency ratio of strong versus weak events). Moreover, the thermodynamic enhancement of atmospheric moisture content is accompanied by a robust increase of TC-related precipitation(3, 8, 12, 14). One of the remaining uncertainties is the expected change in the global number of TCs. Whereas most of the low-resolution global climate models and some SST-forced high resolution atmosphere models project a general decline in the TC frequency(8, 12, 13), other higher resolution models (up to ~50 km) and statistical/dynamical downscaling studies predict an increase(2). There is some evidence to suggest that the TC sensitivity in coupled models depends on the horizontal resolution(3), which underscores further the need to use high-resolution configurations in both atmosphere and ocean.

Resolving mesoscale oceanic features is important for TC sensitivity studies, because strong and slowly propagating TCs are known to enhance vertical ocean mixing, bringing colder subsurface waters to the surface and mixing warm surface waters down to several hundred meters. In some cases, after the passage of a TC, SST can rapidly decrease by up to 10 °C around the area of maximum wind speed(16). Even though the affected area is small [$O(20-100\text{km})$] the surface temperature drop can provide an immediate negative feedback on

the TC development(5). In contrast, a TC-generated and mixing-induced increase of upper ocean heat content (OHC) may be beneficial for the generation of subsequent TCs(17, 18). It has further been suggested that TC-generated ocean mixing may play an important role in the global transport of heat towards the poles(19). We therefore conclude that in order to properly quantify the sensitivity of TCs to greenhouse warming, a coupled modeling approach is necessary that is able to adequately resolve important TC features, such as eyewalls, and oceanic features(20), such as cold wakes, inertial currents, upper ocean mixing and TC-generated mesoscale eddies.

Here, we present results from century-long present-day (PD, with a CO₂ concentration of 367 ppm), CO₂ doubling (2×CO₂, 734 ppm), and CO₂ quadrupling (4×CO₂, 1468 ppm) climate sensitivity experiments conducted with the Community Earth System Model (CESM(21) version 1.2.2) (see Methods for model descriptions). The numerical simulations, which comprise the highest resolution coupled climate change experiments conducted so far, are based on CAM5 with an atmospheric horizontal resolution of approximately 25 km and the POP ocean model with a nominal resolution of 1/10°. These resolutions are sufficient to resolve key mesoscale process, both in the atmosphere and ocean(22). Our study focuses on the simulated CO₂-induced changes in TC frequency, TC-related oceanic wakes, translation speed and landfall characteristics.

Results

Climate response to CO₂ doubling

The PD simulation was integrated for 140 years and the 2×CO₂ and 4×CO₂ experiments are 100 years long. In response to CO₂ doubling and quadrupling global mean surface air temperatures increase towards the end of the simulations by 2.5 °C (1.8 °C) and 5.1 °C (3.8 °C) (Fig. S1A). The top of atmosphere (TOA) radiation imbalance reduces from around 1 W m⁻²

to 0.2 W m^{-2} in the PD experiment (Fig. S1B). Initially there is large radiation imbalance in response to greenhouse gas forcing, but it weakens gradually to around 1 W m^{-2} in the $2\times\text{CO}_2$ and 2 W m^{-2} in the $4\times\text{CO}_2$ experiment, indicating that the coupled system slowly approaches near-equilibrium conditions. However, it is worth noting that a complete equilibration would take up to several hundred years. Global mean precipitation averaged over the last 20 years of the simulations increases by 3.8 % and 7.1 % for the $2\times\text{CO}_2$ and $4\times\text{CO}_2$ experiments relative to the PD climatology (Fig. S1C).

In comparison with other earth system models, the high resolution PD experiment presented here shows substantial improvement in the representation of SST and precipitation (Figs. S2 and S3). Moreover the simulations are able to capture small-scale air-sea interactions partly due to a more realistic representation of oceanic frontal zones, mesoscale ocean eddies (Fig. S4), topography as well as coastal processes. In spite of these improvements, there are still persistent warm biases over the tropical western Pacific Ocean and in high-latitude regions as well as cold biases over the tropical Atlantic (Fig. S2), some of which are similar to those found in low resolution versions of the CESM(22, 23). The PD simulation has an improved representation of the Intertropical Convergence Zone (ITCZ) especially over the eastern Pacific (Fig. S3). But, in comparison with the Tropical Rainfall Measurement Mission (TRMM)(24) observational database, the simulated ITCZ precipitation is too intense and the convergence zone is very narrow, likely due to excessive low-level convergence(6). Furthermore, our PD simulation exhibits a more realistic representation of regional precipitation over major storm track regions, the East Asian summer monsoon, and steep topographic regions such as foothills of Himalayas (Fig. S3).

TC genesis location and tracks

Our TC analysis focuses on the last 20 years of each simulation. To identify genesis locations and tracks of TC, we use instantaneous 6 hourly surface pressure, 10 m wind speed, and surface vorticity data and cut-off criteria, that are similar to those employed in recently developed algorithms (6) (6) (6) (Methods). Comparison of the PD simulation with the observed best track data from the International Best Track Archive for Climate Stewardship Version 4 (IBTrACS4) (25, 26) documents that the high resolution CESM captures the major genesis locations, tracks and densities over the western North Pacific, North Atlantic, eastern Pacific, south Indian Ocean, and South Pacific reasonably well (Fig. 1). However, in terms of TC frequency, we find an underestimation in the model over the western North Pacific, eastern Pacific, and North Atlantic and an overestimation of activity over the central tropical Pacific near the dateline due to ITCZ biases, similar to what has been reported from previous high-resolution modeling studies (6, 12, 22). In spite of these seasonally modulated biases the model provides a reasonable representation of basin-scale climatologies in Indian Ocean and the Pacific (Fig. S5), including the number of TCs per year, mean duration, travel distance, translation speed, and intensity (Table S1).

In response to CO₂ doubling the model simulates a decreased TC track density over almost the entire tropical and subtropical regions (with the exception of the eastern Bay of Bengal, and patches in the Coral and Philippine Seas). This change resembles the observed trend in TC density (Fig. 1C) suggesting that global warming pattern is already emerged in the observation. In the 4×CO₂ experiment, the reduction in TC density is more pronounced extending further into the subtropics (Fig. 1E). TC track density decreases globally by 7 % and 32 % in the 2×CO₂ and 4×CO₂ experiments, respectively. This result is qualitatively consistent with previous studies using of high-resolution (20–50 km) SST-forced pseudo-global warming simulations (9-13). However, it is important to note there that are still remaining modeling uncertainties in the projected response of global TC numbers. Other fully coupled modeling

studies using e.g. the HiFLOR set-up(3) show no significant response of global TC frequencies to increasing CO₂ concentrations but a decrease, when observed SSTs are nudged into the same model(3).

The reduction of TC density in parts of the tropics (Figs. 1D,E) can be explained in terms of the simulated changes in relative humidity and vertical velocity (Fig. 2). Less favorable environmental conditions for TC genesis, in particular a reduction of relative humidity and anomalous downward motion (Fig. 2A), can be linked to an overall weakening of the rising branches of the summer hemispheric Hadley cells (Fig. 2B,C), in agreement with recent studies(27-29). Contrasting the tropical TC suppression, our CO₂ perturbation experiments simulate an increase in TC track densities in higher latitudes, namely east of Japan and along the east coast of North America (Fig. 1D,E). This feature is related to the overall expansion of the subtropics in response to greenhouse warming and the associated poleward shift of the storm tracks(30).

Given that extratropical TCs are typically characterized by higher translation speeds(31), an increase in extratropical TC density (Fig. 1D,E) may also translate into an increase in averaged translation speeds. Our PD simulation captures the overall distribution of the translation speeds in good agreement with the observations (Fig. S6A). However, the mean translation speed is slightly overestimated (Table S1). In our simulations we find an increase of the average translation speed by 2.1 % and 10.9 % in the 2×CO₂ and 4×CO₂ experiments, respectively. Furthermore, the probability distribution of translation speed also changes its shape, exhibiting a decrease in the number of slow-moving TCs and a marked increase of TCs with translation speeds > 40 km h⁻¹ (Fig. S6A). This shift of the distribution can be attributed to the increased TC density poleward of 30 °S and 30 °N (Fig. S6B) simulated in the 2×CO₂ and 4×CO₂ experiments.

Effect of air-sea coupling

TCs extract energy from the surface ocean in the form of sensible and latent heat fluxes that result from strong wind speeds. During the passage of a TC and when ocean mixed layers are relatively shallow, the surface ocean can cool considerably around the TC core due to the entrainment of cold subsurface waters into the mixed layer(32). The TC-induced local SST reduction, referred to as “cold wake”, can further influence the development and lifecycle of the TCs. Moreover, it has been widely recognized that OHC is an important predictor for TC development and intensity(33-35), thereby underscoring the relevance of two-way air-sea interactions. Our current model set-up with $1/10^\circ$ ocean resolution allows us to study the TC sensitivity to greenhouse warming in the presence of such highly localized atmosphere-ocean coupling. To illustrate the upper ocean temperature response to the passage of a TC, we select a typical western North Pacific event which occurred between July 6 to July 18 in model year 124 of the PD simulation (Fig. 3). The TC first moves slowly with a translation speed of about 5 km h^{-1} until it reaches 19°N . Thereafter the translation speed accelerates to about $10\text{--}15 \text{ km h}^{-1}$ in the region between $20\text{--}30^\circ\text{N}$. The maximum wind speed reaches 51 m s^{-1} around the well-resolved edge of the TC which corresponds to a category 3 event based on the Saffier-Simpson scale for 1-minute maximum sustained winds (Fig. 3A). The strong surface winds cool the upper ocean by up to 5°C preferentially along the right side of the track (Fig. 3E). This is where we observe also the strongest drop in OHC (Fig. 3F). The enhanced ocean response to the right of the TC track in the Northern Hemisphere occurs because the asymmetric wind stress provides nearly resonant forcing with inertial ocean currents which intensify entrainment of deeper colder water(32). The latent heat flux anomalies (Fig. 3C), which attain values of up to 1000 W m^{-2} , are stronger on the left side of the track, because negative SST anomalies are less pronounced there. The simulated precipitation shows the characteristic shape of spiraling rain bands (Fig. 3B).

To further examine TC-related changes in ocean thermodynamics, we identify SST cold wakes as the minimum SST anomaly within a period of 5 days after the TC passage and within a 200 km radius. The SST anomaly is calculated by subtracting the previous 14-day average. The strongest TC-induced ocean cooling in our PD simulation attains extreme values of $-15\text{ }^{\circ}\text{C}$. Overall the simulated cold wake amplitudes are similar to observational estimates³⁷ (~ -5 to $-10\text{ }^{\circ}\text{C}$), especially in the more stratified continental shelf regions(16, 36-38) (Table S2). It should be noted here that lower resolution ocean models(34, 39) show considerably weaker cold wakes of typically less than -1 to $-2\text{ }^{\circ}\text{C}$.

Cold wakes, which can be found in the western North Pacific, southern Indian Ocean, eastern Pacific, and South Pacific, are most strongly pronounced for slowly propagating TC over tropical and subtropical regions within $25\text{ }^{\circ}\text{S}$ to $25\text{ }^{\circ}\text{N}$ (Fig. 4A). We also find a secondary peak in cold wake amplitude around $40\text{ }^{\circ}\text{N}$ where most of the storms have high translation speeds that can exceed 30 km h^{-1} (Fig. 4B). The relationship between TC intensity and SST cooling for different TC translation speeds remains essentially unaltered for the $2\times\text{CO}_2$ and $4\times\text{CO}_2$ experiments (Fig. S7). Our $4\times\text{CO}_2$ perturbation experiment shows a discernable decrease in the annually accumulated tropical ocean surface cooling induced by TCs (Fig. 5), which can be attributed to the overall reduction in TC frequencies. An enhanced cold wake effect poleward of $40\text{ }^{\circ}\text{N}$ in the North Atlantic can be explained in terms of the simulated meridional extension of the TC tracks (Figs. 1D,E).

Landfalling TCs

One of the key advantages of a mesoscale-resolving coupled model is its capability to resolve weather and climate processes in mountainous areas and along complex coastlines more accurately. To determine the future impact of TCs on heavily populated coastlines we identify the TC landfall locations in PD, $2\times\text{CO}_2$ and $4\times\text{CO}_2$, as well as the corresponding

changes in TC intensity and accumulated rainfall (Fig. 6). Considering the realistic representation of TC climatologies in the Indian Ocean and western Pacific equatorward of 30 °S to 30 °N (Fig. S5), we focus on this area for our landfall analysis. A landfalling TC occurs when the land fraction at a previous timestep is 0 and land fraction at the current time step is greater than 0. Based on this algorithm, the locations of landfalling TCs especially along the coastlines and many Indian Ocean and Western Pacific islands are well captured (Fig. 6B). The TC intensity and precipitation during landfall are calculated from the maximum wind speed within a 100 km radius from the storm center and the corresponding area-averaged precipitation. Averaged over the landfalling events, mean wind speed increases by 2.0 % and 6.1 % for the 2×CO₂ and 4×CO₂ experiments, respectively (Fig. S9A). The projected changes in landfalling TC intensity is mainly due to the reduction of the number of weak TCs and an increase of category 3–5 events (Fig. 6E). Precipitation changes are even more pronounced attaining corresponding median values of 21 % and 47 % (Fig. 6F). Even though TC frequencies are projected to decrease, our simulations document that landfalling TCs will be more impactful due to stronger winds and heavier precipitation. We note that the overall trends of TC intensity and precipitation diagnosed for landfalling TCs are qualitatively similar to those for all TCs including non landfalling events (Fig. S9C,D).

Discussion

Previous studies(2, 4, 39) have emphasized the need to use coupled mesoscale-resolving global atmosphere/ocean models in projecting the sensitivity of TCs to future climate change. Our results which are based on one of the highest-resolution coupled global model simulations of long-term future climate change conducted so far, provide new insights into the robustness of previously identified mechanisms. Our model simulates a global reduction of TCs in response to greenhouse warming (Fig. 1D,E, Table S1), thus adding an additional

coupled modelling perspective to an otherwise controversial issue(2, 3). The corresponding spatial pattern shows qualitative similarities with the observed trends(1) (Fig. 1C), thereby lending further support to the simulated response and the notion of already emergent observational changes. The simulated TC reduction in large swaths of the tropics and an extension of the “forbidden near equatorial zone” in the western tropical Pacific (Fig. 6) can be explained by a weakening of the ascending branch of the summer Hadley cells in both hemispheres (Fig. 2) and associated changes in relative humidity and vertical motion (Fig. 2). The results are consistent with the recently identified observational linkage between Hadley cell and TC trends(27) and previous modeling studies that emphasize the role of large-scale tropical atmospheric changes as a controlling factor for future changes in TC development (40-42). The Hadley cell-induced suppression of TCs densities in $4\times\text{CO}_2$ equatorward of 20 degrees latitude (Fig. 2) includes a reduction of slow moving TCs, which in turn leads to a weakening of the aggregated cold wake effect (Fig. 5) and a drop in TC-related ocean mixing.

The coupled model simulations presented here further support the robustness of the previously identified increase in the global number of category 3–5 TCs(3, 10) (Fig 6E). However, the 2.0 % increase in the magnitude of maximum wind speed from doubling CO_2 simulation (Fig. S8) is at the lower end of the expected changes from the Intergovernmental Panel on Climate Change (IPCC) A1B future warming scenario (+2 to +11 %) ², and smaller than projections from the HiFLOR simulations (+3.2 % to 9.0 %)(14). Interestingly, the projected changes in landfalling TC intensity are nonlinear with a massive 150 % increase of category 3–5 events occurring for the first CO_2 doubling (Fig. 6E), but no further change occurring between doubling and quadrupling. The statistical robustness of this saturation effect needs to be further explored in subsequent studies and for different model configurations.

One of the most robust projections(14, 43) of future TC impacts is related to the largely thermodynamically-controlled intensification of rainfall. This process is connected to an

increased risk for coastal flooding. In the $2\times\text{CO}_2$ and $4\times\text{CO}_2$ experiments the increase of tropical SST (averaged over 30°S to 30°N) by 1.8°C and 3.7°C is accompanied by an increase of TC precipitation by 7.7% and 9.5% per degree warming, respectively. This increase slightly outpaces the rates expected from the thermodynamic Clausius Clapeyron scaling ($\sim 7\%^\circ\text{C}^{-1}$). This result is consistent with earlier reports suggesting that future TC precipitation is controlled by both the increases in environmental water vapor as well as storm intensity(2, 14)

Even though our high-resolution coupled simulations exhibit reduced tropical SST biases, in comparison with coarser resolution coupled general circulation models, the mesoscale resolving CESM1.2.2 PD simulation still exhibits substantial offsets in TC densities and tracks (Fig. S5), in particular for North Atlantic hurricanes. A more detailed analysis is necessary to ascertain the role of biases in convection and the representation of easterly waves and tropical Atlantic SST errors (Fig. S2). A viable approach to overcome the potential effects of SST biases on TC genesis and tracks under PD conditions would be to use SST nudging techniques that tie the simulated SST closer to the observations(3). However, it remains unclear to what extent such methods can be applied for stronger CO_2 perturbations, such as for CO_2 quadrupling.

Summarizing, our mesoscale-resolving coupled CO_2 perturbation experiments confirm some well-known features of the sensitivity of TCs to greenhouse warming. We therefore conclude that the two-way air sea interaction and the effects of ocean mesoscale processes do not play major roles in large-scale shifts in TC statistics. However, we find several new features, such as the reduction of aggregated TC ocean cooling and associated mixing equatorward of 20 degrees latitude (Fig. 5), as well as saturation in wind intensity for CO_2 quadrupling (Fig. 6E) that highlight the added value of improved representations of mesoscale air-sea coupling and coastal and topographic processes.

Methods

Model and computational descriptions

In the present study, the Community Earth System Model(21) version 1.2.2 (CESM1.2.2) is employed to perform fully coupled ultra-high-resolution simulations. The atmosphere component is the Community Atmosphere Model (CAM5)(44) with a spectral element dynamic core at a horizontal resolution of around 0.25° and 30 vertical layers. CAM5 is able to capture TCs and observed behavior of global accumulated cyclone energy, albeit with large basin-to-basin differences in TC climatologies(6) (Fig. S5). The ocean component of CESM is the Parallel Ocean Program version 2 (POP2)(45) whichh is configured with a horizontal resolution of 0.1° (decreasing from 11 km at the Equator to 2.5 km at high latitudes) and 62 vertical levels. The land model is the Community Land Model version 4 (CLM4)(46) and the sea-ice component is the Community Ice Code version 4 (CICE4)(47). The prognostic carbon-nitrogen cycle component was turned off in our simulations. The configuration for our PD experiment is very similar to the one used in (22) except that we adjusted some elements of the convection scheme to improve our PD representation of the El Niño-Southern Oscillation. The high-resolution CESM1.2.2 model shows a substantial mean-state bias reduction in SST (Fig. S2) and is capable of capturing localized small-scale phenomena such as air-sea interactions over ocean frontal zones, mesoscale ocean eddies (Fig. S4), and atmospheric extremes including eye-walled TCs and convective systems generated by the Rockies(22).

We conduct three experiments with different levels of fixed greenhouse gas conditions: (1) PD with a CO_2 concentration of 367 ppm), (2) CO_2 doubling ($2\times\text{CO}_2$, 734 ppm), and (3) CO_2 quadrupling ($4\times\text{CO}_2$, 1468 ppm). All other greenhouse gas and aerosol concentrations have been kept at PD levels. The PD simulation is initialized from a quasi-equilibrated climate state(22) and was then integrated for another 140 years. The doubling and quadrupling CO_2 forcing experiments were branched off from year 71 of the PD experiment and integrated for

100 years each. For the TC analysis, we focus on the better equilibrated last the 20 years of each simulation. Unless otherwise stated, all other variables used in the main text focus on the last 20 years of each simulation.

TC detection and track

TCs are detected and tracked by adopting (with some minor adjustments) a recently proposed method⁴. For our detection we use 6-hourly instantaneous surface pressure, 10-m wind speed, and surface vorticity. First, we identify candidate lows by calculating local surface pressure anomaly minima (threshold: lower than -3 hPa). Surface pressure anomalies (PS') are obtained by subtracting surface pressure from a 14-day retrospective mean $PS'_t = PS_t - [PS]_{(-14d,-1d)}$ where the square bracket denotes a time average. If the maximum 10-m wind speed within 100 km radius from the local pressure minimum does not exceeds 10 m s^{-1} , the low is discarded. After finding candidate lows at all time steps, we employ tracking over 6 hourly intervals. The next track location at $t+6\text{h}$ is chosen simply as the nearest low to the original low at time t . If another low is located within a 400 km radius circle, the track is continued. At subsequent time step ($t+12\text{h}$), the low closest to the location that is extrapolated between t and $t+6\text{h}$ is chosen to be the next track. If no other low is located within a 400 km radius circle, the track is terminated. This scheme is almost the same as the original method(6), except they use 3 hourly instantaneous data, 200 km radius for tracks, and a 50 km radius for wind speed. To avoid multiple counting of single storms, we additionally remove any duplicated tracks and keep the track that started earliest. In addition, if the maxima of wind speed along the track never reaches 17 m s^{-1} , which is the threshold for a tropical storm on the Saffier-Simpson scale, and the duration of the storm is less than 2 days, the track is also eliminated. Lastly, we impose a threshold value of 0.00145 s^{-1} for surface vorticity magnitude along the track to obtain global TC numbers of around 85 per year, similar to the observations.

Translation speed

The translation speed is calculated based on the great circle distance of two points between that at 6 hours before and 6 hours after the current location and then divided by 12 hours. Translation speed at initial and final positions is calculated using the two neighboring forward and backward positions, respectively.

Upper ocean heat contents

Following the previous study(48), the Ocean heat content (OHC) is defined here as

$$OHC = \rho_o C_p \int_{Z_{26}}^0 [T(z) - 26] dz \quad (1)$$

where ρ_o is sea water density ($\rho_o=1025 \text{ kg m}^{-3}$), C_p is ocean heat capacity ($C_p= 4.0 \times 10^3 \text{ J kg}^{-1} \text{ }^\circ\text{C}^{-1}$), $T(z)$ the ocean temperature as a function of depth z down to the $26 \text{ }^\circ\text{C}$ isotherm, Z_{26} . The reference depth Z_{26} is the climatological depth during the respective TC season. For the TC case over the western North Pacific (Fig. 3), the climatological Z_{26} is calculated during June to October. Note that the existence of a $26 \text{ }^\circ\text{C}$ isotherm is a necessary condition for TC formation (49).

References

- 1 Murakami, H. *et al.* Detected climatic change in global distribution of tropical cyclones. *Proceedings of the National Academy of Sciences*, 201922500, doi:10.1073/pnas.1922500117 (2020).
- 2 Knutson, T. R. *et al.* Tropical cyclones and climate change. *Nature Geoscience* **3**, 157-163, doi:10.1038/ngeo779 (2010).
- 3 Vecchi, G. A. *et al.* Tropical cyclone sensitivities to CO2 doubling: roles of atmospheric resolution, synoptic variability and background climate changes. *Climate Dynamics* **53**, 5999-6033, doi:10.1007/s00382-019-04913-y (2019).
- 4 Li, H. & Sriver, R. L. Effects of ocean grid resolution on tropical cyclone-induced upper ocean responses using a global ocean general circulation model. *Journal of Geophysical Research: Oceans* **121**, 8305-8319, doi:10.1002/2016jc011951 (2016).
- 5 Li, H. & Sriver, R. L. Impact of air–sea coupling on the simulated global tropical cyclone activity in the high-resolution Community Earth System Model (CESM). *Climate Dynamics* **53**, 3731-3750, doi:10.1007/s00382-019-04739-8 (2019).
- 6 Bacmeister, J. T. *et al.* Exploratory High-Resolution Climate Simulations using the Community Atmosphere Model (CAM). *Journal of Climate* **27**, 3073-3099, doi:10.1175/jcli-d-13-00387.1 (2014).
- 7 Reed, K. A. *et al.* Impact of the dynamical core on the direct simulation of tropical cyclones in a high-resolution global model. *Geophysical Research Letters* **42**, 3603-3608, doi:10.1002/2015gl063974 (2015).
- 8 Gettelman, A., Bresch, D. N., Chen, C. C., Truesdale, J. E. & Bacmeister, J. T. Projections of future tropical cyclone damage with a high-resolution global climate model. *Climatic Change* **146**, 575-585, doi:10.1007/s10584-017-1902-7 (2018).
- 9 Murakami, H., Mizuta, R. & Shindo, E. Future changes in tropical cyclone activity projected by multi-physics and multi-SST ensemble experiments using the 60-km-mesh MRI-AGCM. *Climate Dynamics* **39**, 2569-2584, doi:10.1007/s00382-011-1223-x (2012).
- 10 Murakami, H. *et al.* Future Changes in Tropical Cyclone Activity Projected by the New High-Resolution MRI-AGCM. *Journal of Climate* **25**, 3237-3260, doi:10.1175/jcli-d-11-00415.1 (2012).
- 11 Murakami, H., Hsu, P.-C., Arakawa, O. & Li, T. Influence of Model Biases on Projected Future Changes in Tropical Cyclone Frequency of Occurrence. *Journal of Climate* **27**, 2159-2181, doi:10.1175/jcli-d-13-00436.1 (2014).
- 12 Bacmeister, J. T. *et al.* Projected changes in tropical cyclone activity under future warming scenarios using a high-resolution climate model. *Climatic Change* **146**, 547-560, doi:10.1007/s10584-016-1750-x (2018).
- 13 Wehner, M. F., Reed, K. A., Loring, B., Stone, D. & Krishnan, H. Changes in tropical cyclones under stabilized 1.5 and 2.0 °C global warming scenarios as simulated by the Community Atmospheric Model under the HAPPI protocols. *Earth Syst. Dynam.* **9**, 187-195, doi:10.5194/esd-9-187-2018 (2018).
- 14 Liu, M., Vecchi, G. A., Smith, J. A. & Knutson, T. R. Causes of large projected increases in hurricane precipitation rates with global warming. *npj Climate and Atmospheric Science* **2**, 38, doi:10.1038/s41612-019-0095-3 (2019).
- 15 Kim, H.-S. *et al.* Tropical Cyclone Simulation and Response to CO2 Doubling in the GFDL CM2.5 High-Resolution Coupled Climate Model. *Journal of Climate* **27**, 8034-8054, doi:10.1175/jcli-d-13-00475.1 (2014).
- 16 Chiang, T.-L., Wu, C.-R. & Oey, L.-Y. Typhoon Kai-Tak: An Ocean's Perfect Storm. *Journal of Physical Oceanography* **41**, 221-233, doi:10.1175/2010jpo4518.1 (2011).

- 17 Park, M.-S., Elsberry, R. L. & Harr, P. A. Vertical Wind Shear and Ocean Heat Content as Environmental Modulators of Western North Pacific Tropical Cyclone Intensification and Decay. *Tropical Cyclone Research and Review* **1**, 448-457, doi:<https://doi.org/10.6057/2012TCRR04.03> (2012).
- 18 Trenberth, K. E., Cheng, L., Jacobs, P., Zhang, Y. & Fasullo, J. Hurricane Harvey Links to Ocean Heat Content and Climate Change Adaptation. *Earth's Future* **6**, 730-744, doi:10.1029/2018ef000825 (2018).
- 19 Sriver, R. L. & Huber, M. Observational evidence for an ocean heat pump induced by tropical cyclones. *Nature* **447**, 577-580, doi:10.1038/nature05785 (2007).
- 20 Zarzycki, C. M. Tropical Cyclone Intensity Errors Associated with Lack of Two-Way Ocean Coupling in High-Resolution Global Simulations. *Journal of Climate* **29**, 8589-8610, doi:10.1175/jcli-d-16-0273.1 (2016).
- 21 Hurrell, J. W. *et al.* The Community Earth System Model: A Framework for Collaborative Research. *Bulletin of the American Meteorological Society* **94**, 1339-1360, doi:10.1175/bams-d-12-00121.1 (2013).
- 22 Small, R. J. *et al.* A new synoptic scale resolving global climate simulation using the Community Earth System Model. *Journal of Advances in Modeling Earth Systems* **6**, 1065-1094, doi:10.1002/2014ms000363 (2014).
- 23 McClean, J. L. *et al.* A prototype two-decade fully-coupled fine-resolution CCSM simulation. *Ocean Modelling* **39**, 10-30, doi:<https://doi.org/10.1016/j.ocemod.2011.02.011> (2011).
- 24 Huffman, G. J. *et al.* The TRMM Multisatellite Precipitation Analysis (TMPA): Quasi-Global, Multiyear, Combined-Sensor Precipitation Estimates at Fine Scales. *Journal of Hydrometeorology* **8**, 38-55, doi:10.1175/jhm560.1 (2007).
- 25 Knapp, K. R., Diamond, H. J., Kossin, J. P., Kruk, M. C. & Schreck, C. J. I. International Best Track Archive for Climate Stewardship (IBTrACS) Project, Version 4. *NOAA National Centers for Environmental Information*. (<https://doi.org/10.25921/82ty-9e16>) (2018).
- 26 Knapp, K. R., Kruk, M. C., Levinson, D. H., Diamond, H. J. & Neumann, C. J. The International Best Track Archive for Climate Stewardship (IBTrACS). *Bulletin of the American Meteorological Society* **91**, 363-376, doi:10.1175/2009bams2755.1 (2010).
- 27 Sharmila, S. & Walsh, K. J. E. Recent poleward shift of tropical cyclone formation linked to Hadley cell expansion. *Nature Climate Change* **8**, 730-736, doi:10.1038/s41558-018-0227-5 (2018).
- 28 Studholme, J. & Gulev, S. Concurrent Changes to Hadley Circulation and the Meridional Distribution of Tropical Cyclones. *Journal of Climate* **31**, 4367-4389, doi:10.1175/jcli-d-17-0852.1 (2018).
- 29 Held, I. M. & Zhao, M. The Response of Tropical Cyclone Statistics to an Increase in CO₂ with Fixed Sea Surface Temperatures. *Journal of Climate* **24**, 5353-5364, doi:10.1175/jcli-d-11-00050.1 (2011).
- 30 Bengtsson, L., Hodges, K. I. & Roeckner, E. Storm Tracks and Climate Change. *Journal of Climate* **19**, 3518-3543, doi:10.1175/jcli3815.1 (2006).
- 31 Moon, I.-J., Kim, S.-H. & Chan, J. C. L. Climate change and tropical cyclone trend. *Nature* **570**, E3-E5, doi:10.1038/s41586-019-1222-3 (2019).
- 32 Price, J. F. Upper Ocean Response to a Hurricane. *Journal of Physical Oceanography* **11**, 153-175, doi:10.1175/1520-0485(1981)011<0153:Uortah>2.0.Co;2 (1981).
- 33 Emanuel, K. A. Thermodynamic control of hurricane intensity. *Nature* **401**, 665-669, doi:10.1038/44326 (1999).

- 34 Lloyd, I. D. & Vecchi, G. A. Observational Evidence for Oceanic Controls on Hurricane Intensity. *Journal of Climate* **24**, 1138-1153, doi:10.1175/2010jcli3763.1 (2011).
- 35 Vincent, E. M., Emanuel, K. A., Lengaigne, M., Vialard, J. & Madec, G. Influence of upper ocean stratification interannual variability on tropical cyclones. *Journal of Advances in Modeling Earth Systems* **6**, 680-699, doi:10.1002/2014ms000327 (2014).
- 36 Park, J.-H. *et al.* Rapid Decay of Slowly Moving Typhoon Soulik (2018) due to Interactions With the Strongly Stratified Northern East China Sea. *Geophysical Research Letters* **46**, 14595-14603, doi:10.1029/2019gl086274 (2019).
- 37 D'Asaro, E. A. *et al.* Impact of Typhoons on the Ocean in the Pacific. *Bulletin of the American Meteorological Society* **95**, 1405-1418, doi:10.1175/bams-d-12-00104.1 (2014).
- 38 Wada, A., Uehara, T. & Ishizaki, S. Typhoon-induced sea surface cooling during the 2011 and 2012 typhoon seasons: observational evidence and numerical investigations of the sea surface cooling effect using typhoon simulations. *Progress in Earth and Planetary Science* **1**, 11, doi:10.1186/2197-4284-1-11 (2014).
- 39 Murakami, H. *et al.* Simulation and Prediction of Category 4 and 5 Hurricanes in the High-Resolution GFDL HiFLOR Coupled Climate Model. *Journal of Climate* **28**, 9058-9079, doi:10.1175/jcli-d-15-0216.1 (2015).
- 40 Sugi, M., Murakami, H. & Yoshimura, J. On the Mechanism of Tropical Cyclone Frequency Changes Due to Global Warming. *Journal of the Meteorological Society of Japan. Ser. II* **90A**, 397-408, doi:10.2151/jmsj.2012-A24 (2012).
- 41 Sugi, M., Noda, A. & Sato, N. Influence of the Global Warming on Tropical Cyclone Climatology: An Experiment with the JMA Global Model. *Journal of the Meteorological Society of Japan. Ser. II* **80**, 249-272, doi:10.2151/jmsj.80.249 (2002).
- 42 Bell, S. S. *et al.* Projections of southern hemisphere tropical cyclone track density using CMIP5 models. *Climate Dynamics* **52**, 6065-6079, doi:10.1007/s00382-018-4497-4 (2019).
- 43 Yoshida, K., Sugi, M., Mizuta, R., Murakami, H. & Ishii, M. Future Changes in Tropical Cyclone Activity in High-Resolution Large-Ensemble Simulations. *Geophysical Research Letters* **44**, 9910-9917, doi:10.1002/2017gl075058 (2017).
- 44 Neale, R. B. *et al.* Description of the NCAR community atmosphere model (CAM 5.0). *NCAR Tech. Note NCAR/TN-4861 STR. Natl. Cent. Atmos. Res., Boulder, Colo.* [Available at http://www.cesm.ucar.edu/models/cesm1.1/cam/docs/description/cam5_desc.pdf] (2010).
- 45 Smith, R. *et al.* The Parallel Ocean Program (POP) reference manual. *Tech. Rep. LAUR-10-01853, Los Alamos Natl. Lab., Los Alamos.* [Available at <http://www.cesm.ucar.edu/models/cesm1.0/pop2/doc/sci/POPRefManual.pdf>] (2010).
- 46 Lawrence, D. M. *et al.* Parameterization improvements and functional and structural advances in Version 4 of the Community Land Model. *Journal of Advances in Modeling Earth Systems* **3**, doi:10.1029/2011ms00045 (2011).
- 47 Hunke, E. C. & Lipscomb, W. H. CICE: The Los Alamos Sea Ice Model. Documentation and Software User's Manual. Version 4.0. T-3 Fluid Dynamics Group, Los Alamos National Laboratory, Tech. Rep. LA-CC-06-012. (2008).
- 48 Leipper, D. F. & Volgenau, D. Hurricane Heat Potential of the Gulf of Mexico. *Journal of Physical Oceanography* **2**, 218-224, doi:10.1175/1520-0485(1972)002<0218:HHPOTG>2.0.CO;2 (1972).
- 49 Palmén, E. On the formation and structure of tropical hurricanes. *Geophysica* **3**, 26-38 (1948).

- 50 Hurrell, J. W., Hack, J. J., Shea, D., Caron, J. M. & Rosinski, J. A New Sea Surface Temperature and Sea Ice Boundary Dataset for the Community Atmosphere Model. *Journal of Climate* **21**, 5145-5153, doi:10.1175/2008jcli2292.1 (2008).
- 51 Ducet, N., Le Traon, P. Y. & Reverdin, G. Global high-resolution mapping of ocean circulation from TOPEX/Poseidon and ERS-1 and -2. *Journal of Geophysical Research: Oceans* **105**, 19477-19498, doi:10.1029/2000jc900063 (2000).

Acknowledgements: This research was supported by the Institute for Basic Science (IBS) IBS-R028-D1. The CESM code is publicly available from the National Center for Atmospheric Research. Figures were generated by the NCAR Command Language (Version 6.4.0) [Software]. (2017). Boulder, Colorado: UCAR/NCAR/CISL/VETS. <http://dx.doi.org/10.5065/D6WD3XH5>. This is IPRC publication X and SOEST contribution Y. The simulations were conducted on the IBS/ICCP supercomputer “*Aleph*”, 1.43 petaflops high-performance Cray XC50-LC Skylake computing system with 18,720 processor cores, 9.59 petabytes storage, and 43 petabytes tape archive space. The throughput for the CESM 1.2.2 model simulations averaged to about 3 model years per day of integration. Further information about the simulations can be found at (<https://ibsclimate.org/research/ultra-high-resolution-climate-simulation-project>). We thank Dr. Justin Small for helpful suggestions in running the CESM1.2.2 high resolution model.

Data Availability: The observed tropical cyclone data are obtained from the International Best Track Archive for Climate Stewardship (IBTrACS; <https://www.ncdc.noaa.gov/ibtracs/index.php?name=ib-v4-access>) Version 4(25, 26). The HadISST(50) can be obtained from UK Meteorological Office, Hadley Centre (<http://www.badc.nerc.ac.uk/data/hadisst>) and the TRMM(24) 3B43 product is from the Goddard Earth Sciences Data and Information Services Center (<http://disc.sci.gsfc.nasa.gov>). SSHA data can be obtained from Archiving Validation and Interpretation of Satellite Oceanographic Data (AVISO)(51) merged product (<http://www.avisio.altimetry.fr>). All CESM1.2.2 model simulation data are available to the scientific community and are provided through a customized data distribution service, which can be accessed after contacting the

This is a non-peer reviewed preprint submitted to EarthArXiv

corresponding authors and filling out a specific data request form available on

<https://ibsclimate.org/research/ultra-high-resolution-climate-simulation-project>.

Supplementary Materials:

Materials and Methods

Figures S1–S8

Tables S1–S2

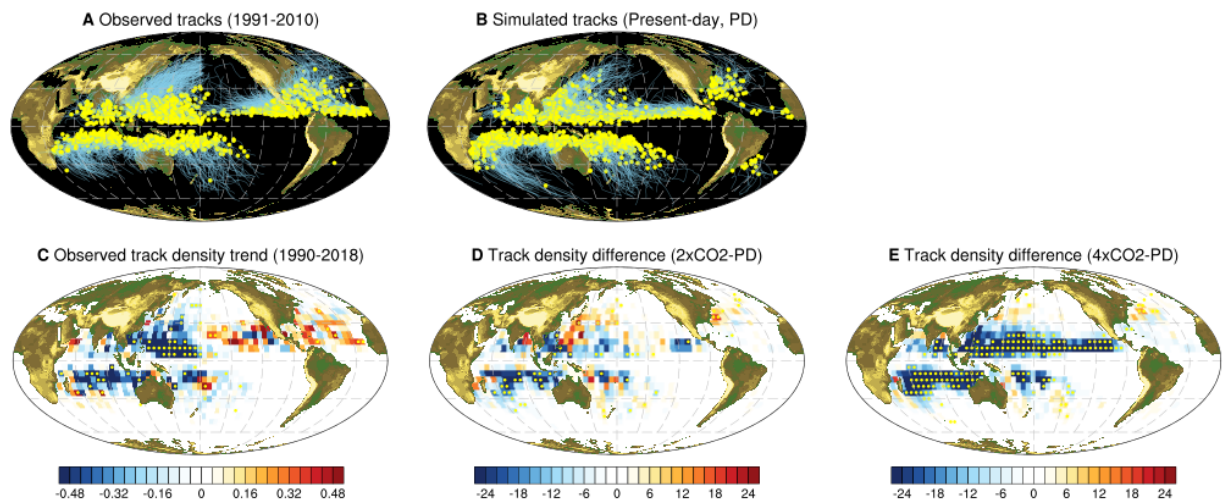


Fig 1. Present-day (PD) and future tropical cyclones (TCs) genesis location and tracks.

(A and B) TC genesis location (yellow dots) and tracks (blue lines) from (A) observations and (B) PD simulation. (C) Linear trend of the observed TC track density (hours day⁻¹/year) for the period 1990 to 2018, (D and E) track density changes (hours day⁻¹) in (D) CO₂ doubling (2×CO₂) and (E) CO₂ quadrupling (4×CO₂) conditions related to PD condition. Observational data is from IBTrACS4 during the 1990-2018 period. Track density was obtained by the number of TC tracks over 5 × 5 degrees grid box. Yellow dotted areas in C-E indicate values for which the local null hypothesis of zero relation can be rejected at the 95 % level based on a Student's *t* test.

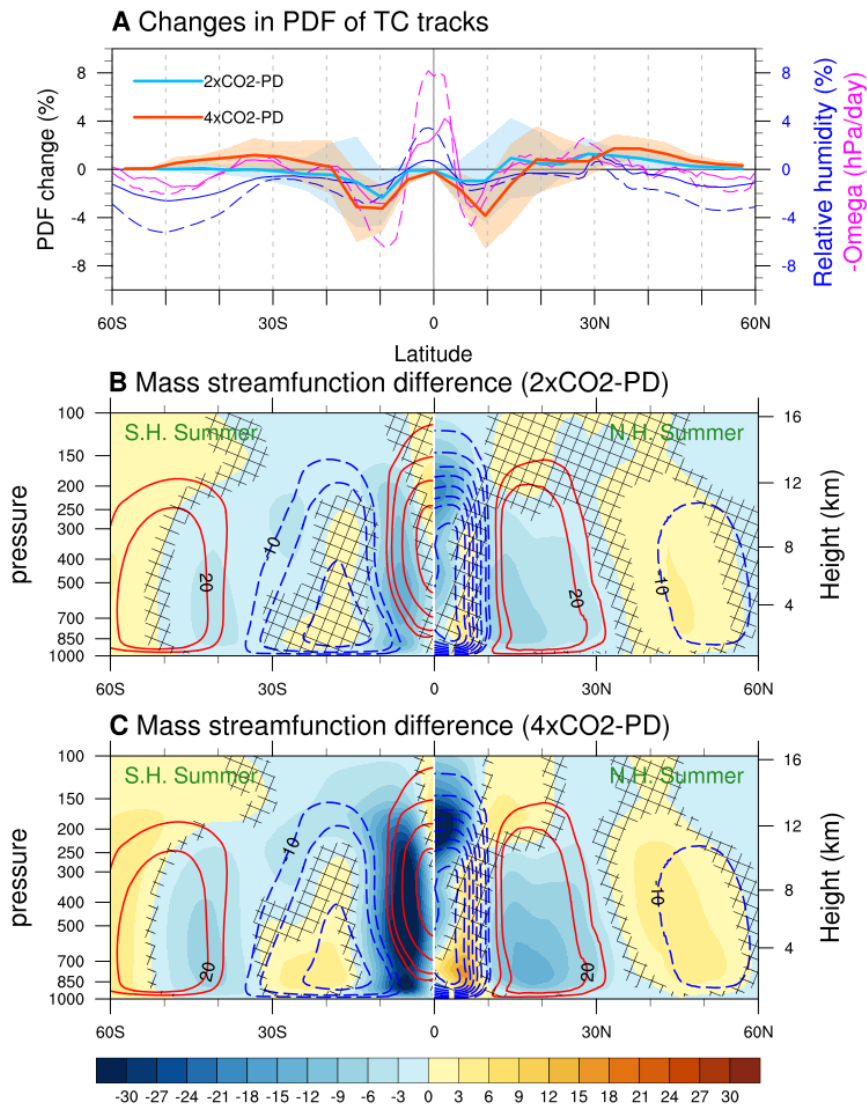


Fig 2. Changes in latitudinal distribution of TC tracks and meridional overturning circulations. (A) Changes in the probability density distribution (PDF) of the TC tracks as a function of latitude in 2×CO₂ (light blue thick line) and 4×CO₂ (red thick line) conditions relative to PD. Annual and zonal mean relative humidity (%) at 700 hPa (blue thin lines) and vertical velocity (hPa day⁻¹) at 500 hPa (magenta thin lines) in 2×CO₂ (solid lines) and 4×CO₂ (dashed lines) conditions. For consistency, the vertical velocity is multiplied by -1. Shadings indicate one standard deviation of the year-to-year PDF for 2×CO₂ (blue) and 4×CO₂ (red) conditions. (B and C) Climatological summertime mass stream function in PD (contours), and changes in mass stream

function (shading) in (B) $2\times\text{CO}_2$ and (C) $4\times\text{CO}_2$ experiments. Summer mean is computed over June-November for the Northern Hemisphere and December-May for the Southern Hemisphere. Values that are not statistically significant at 95 % confidence level are marked by black cross-hatching.

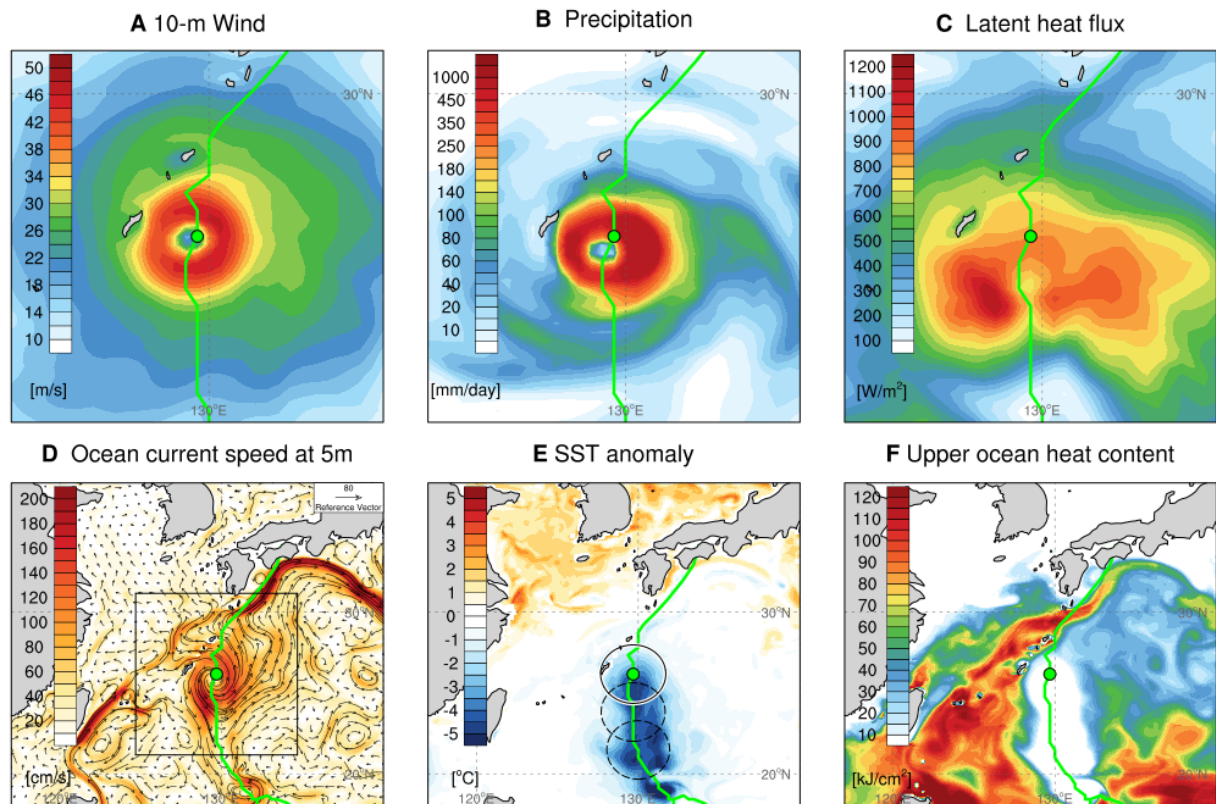


Fig 3. Upper ocean response to the passage of a TC. A snapshot of (A) 10-m wind speed (m s^{-1}), (B) precipitation (mm day^{-1}), (C) latent heat flux (W m^{-2}), (D) ocean current (vector) and its speed (shading) at a depth of 5 m (cm s^{-1}), (E) sea surface temperature (SST, $^{\circ}\text{C}$) anomaly, and (F) upper ocean heat content (OHC, kJ cm^{-2}) in response to a TC case passing over the western North Pacific. The SST anomaly is calculated by subtracting the previous 14-day average. Green line indicates the track of the selected TC and green circle indicates the center of the storm. Black box denotes the zoomed-in area in A-C. The circle with black solid line in (E) represents the 200 km boundary from the storm center that is used to calculate maximum SST cooling (i.e., cold wakes) whereas circles with black dashed lines are those for storms at 24 hours and 48 hours before.

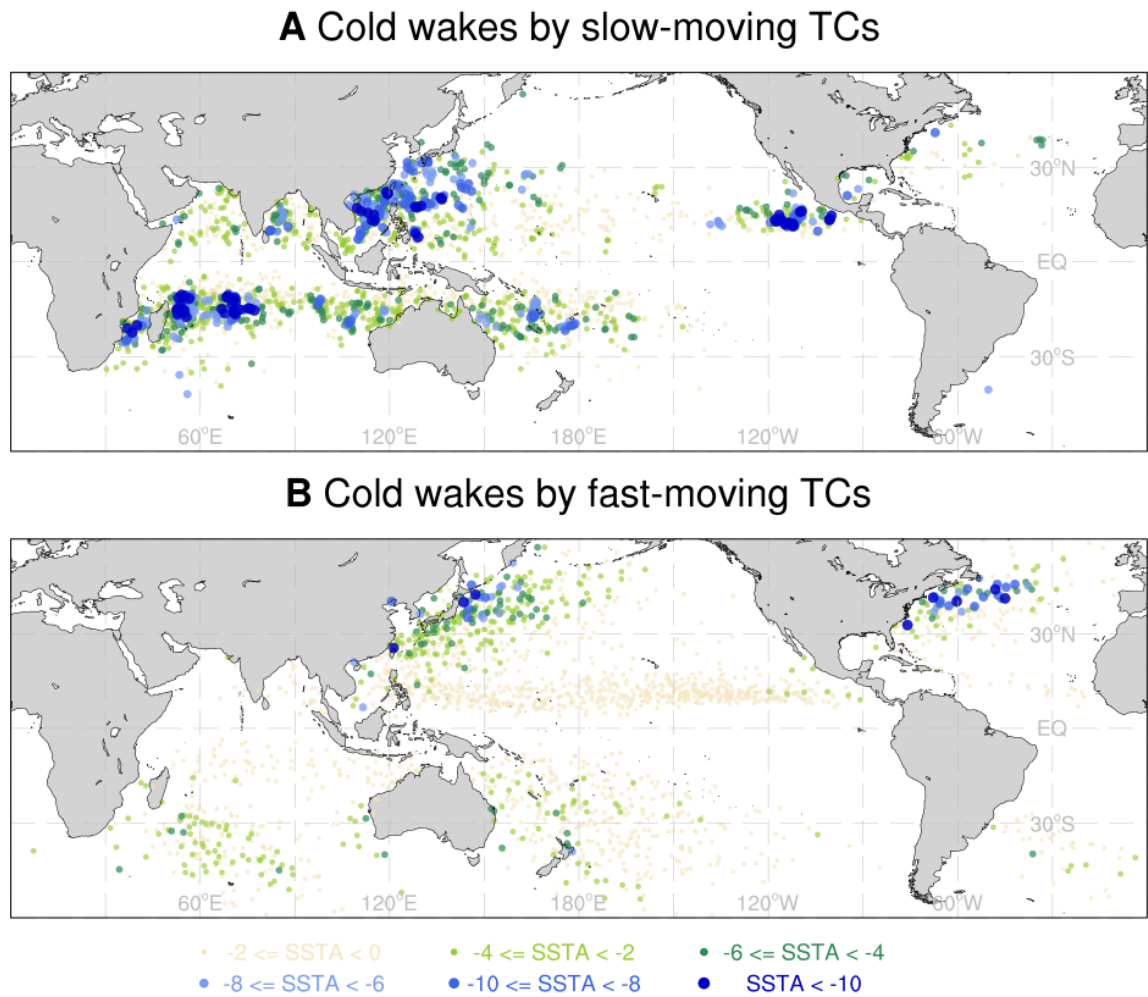


Fig 4. Cold wakes and translation speeds. Global distribution of the TC-induced cold wakes by (A) slow-moving TCs and (B) fast-moving TCs in the PD simulation. Slow-moving TCs are defined as the TCs with translation speed lower than 10 km h^{-1} . Fast-moving TCs are defined as the speed greater than 30 km h^{-1} . The cold wakes are identified as the minimum SST anomaly within a circle of 200 km radius (e.g., circles in Fig. 3E) during the next 5 days after the TC passage.

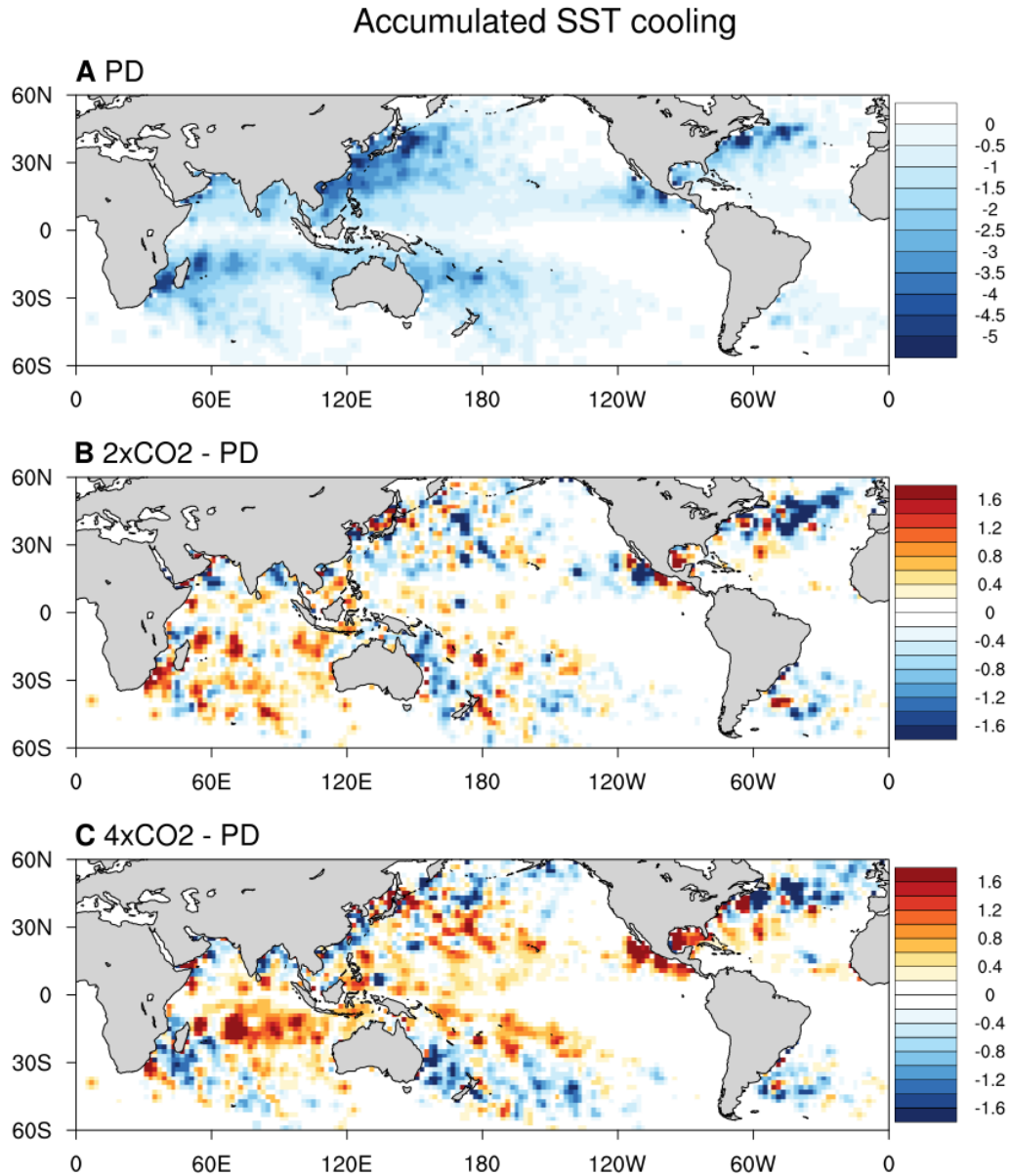


Fig. 5. Accumulated SST cooling effect induced by TC activity. (A) Annually accumulated cooling due to TC passages in the PD experiment. The cooling effect is calculated by adding the SST anomaly within a circle of 200 km radius along the TC passages over a year. (B and C) Changes in SST cooling effect in (B) $2\times\text{CO}_2$ and (C) $4\times\text{CO}_2$ relative to PD. The patterns are interpolated into 2×2 degrees grid box. All fields are smoothed using a nine-point local average weighted by distance from the grid center.

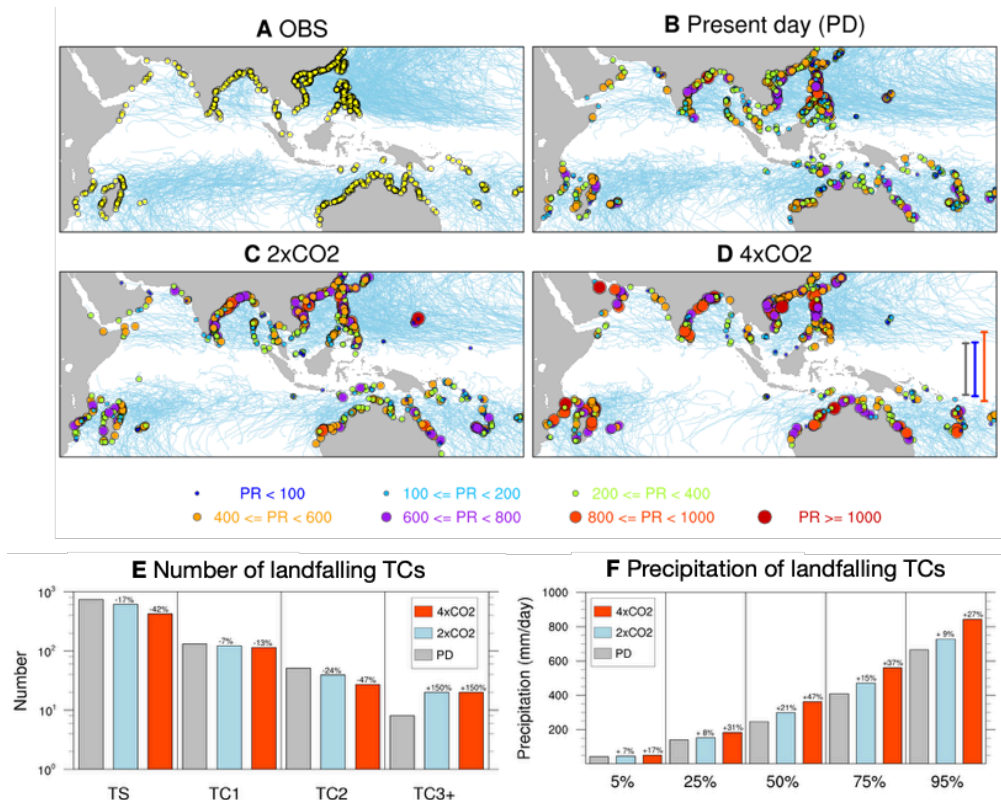


Fig. 6. Locations, precipitation and intensity of landfalling TCs. (A to D) TC tracks (light blue) and landfalling locations (yellow circles) from (A) observation, (B) PD, (C) 2×CO₂, and (D) 4×CO₂ simulations. Colors in B-D indicate different range of precipitation averaged over a circle of 100 km radius from the storm center. (E) The number of landfalling TCs for each category from tropical storm (TS) to TC greater than category 3 (TC3+) based on the Saffier-Simpson scale in PD (gray), 2×CO₂ (blue), and 4×CO₂ (red) conditions. (F) Precipitation (mm day⁻¹) by the landfalling TCs at each percentile of 5 %, 25 %, 50 % (median), 75 %, and 95 %, respectively. Numbers above the bars indicate relative changes in the (E) TC number and (F) precipitation compared to PD values. To remove the impact of extratropical storms, landfalling TCs within 30 °S–30 °N are considered. Vertical bars in D denote the “forbidden near equatorial zone” defined as a longitudinal average of the genesis location nearest to the equator for PD (gray), 2×CO₂ (blue), and 4×CO₂ (red), respectively.

Supplementary Information for

**Tropical cyclone response to anthropogenic warming as
simulated by a mesoscale-resolving global coupled earth system
model**

Jung-Eun Chu, Sun-Seon Lee, Axel Timmermann, Christian Wengel, Malte F. Stuecker,
Ryohei Yamaguchi

Corresponding to: Sun-Seon Lee, Email: sunseonlee@pusan.ac.kr

_____ Axel Timmermann, Email: axel@ibsclimate.org

This PDF file includes the following:

Figs. S1 to S8

Tables S1 to S2

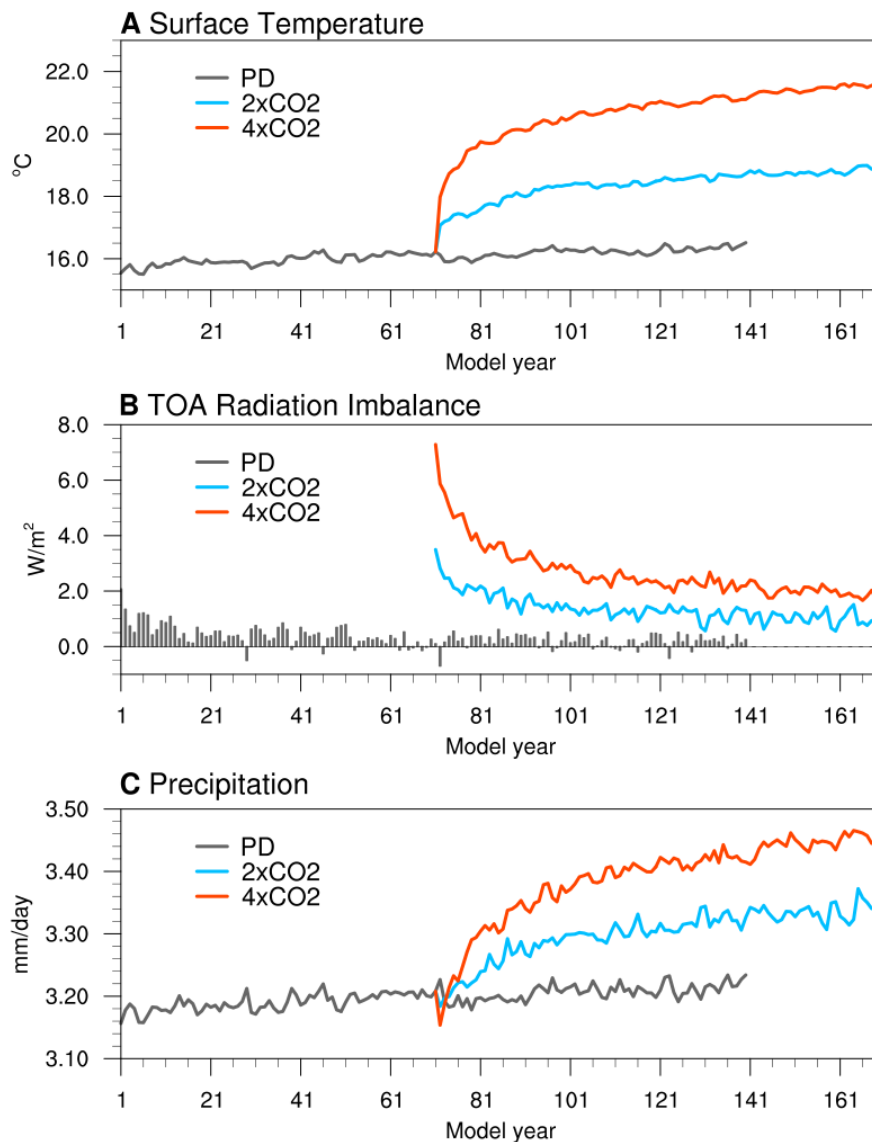


Figure S1. Time series of the global and annual mean (A) surface air temperature ($^{\circ}\text{C}$), (B) net radiation imbalance at top of the atmosphere (TOA) (positive downward, W m^{-2}), and (C) precipitation (mm day^{-1}). Gray colors denote quantities for 140 years of the PD condition, and blue and red lines indicate 100 years of doubling CO_2 ($2\times\text{CO}_2$) and quadrupling CO_2 ($4\times\text{CO}_2$) experiments started from year 71 of PD, respectively.

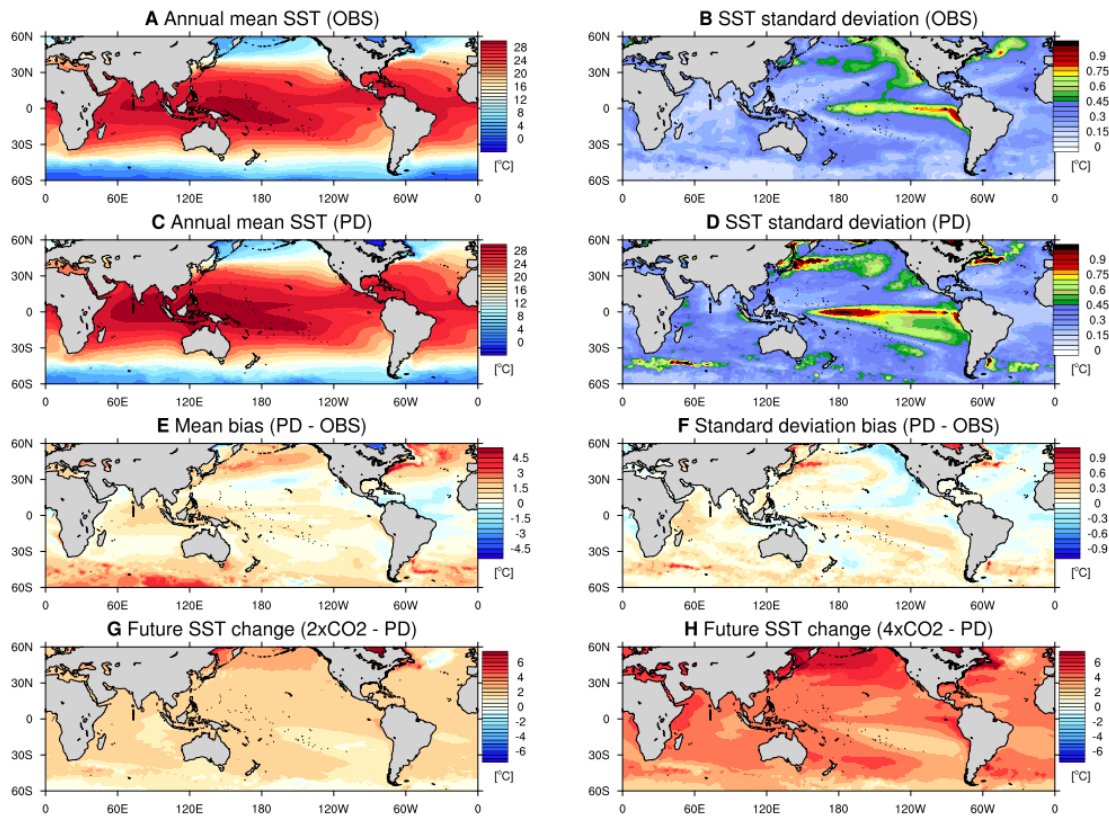


Figure S2. (A and C) Annual mean SST ($^{\circ}\text{C}$) climatology from (A) observation and (C) PD condition. (B and D) Standard deviation of the annual mean SST from (B) observation and (D) PD condition. (E and F) Model bias in (E) annual mean SST and (F) standard deviation. (G and H) Changes in annual mean SST in (G) $2\times\text{CO}_2$ and (H) $4\times\text{CO}_2$ relative to PD. Observational data is from HadISST(50) for the 1990-2018 period. Last 20 years of the simulation data are used. Long-term linear trends were removed before any statistical analysis.

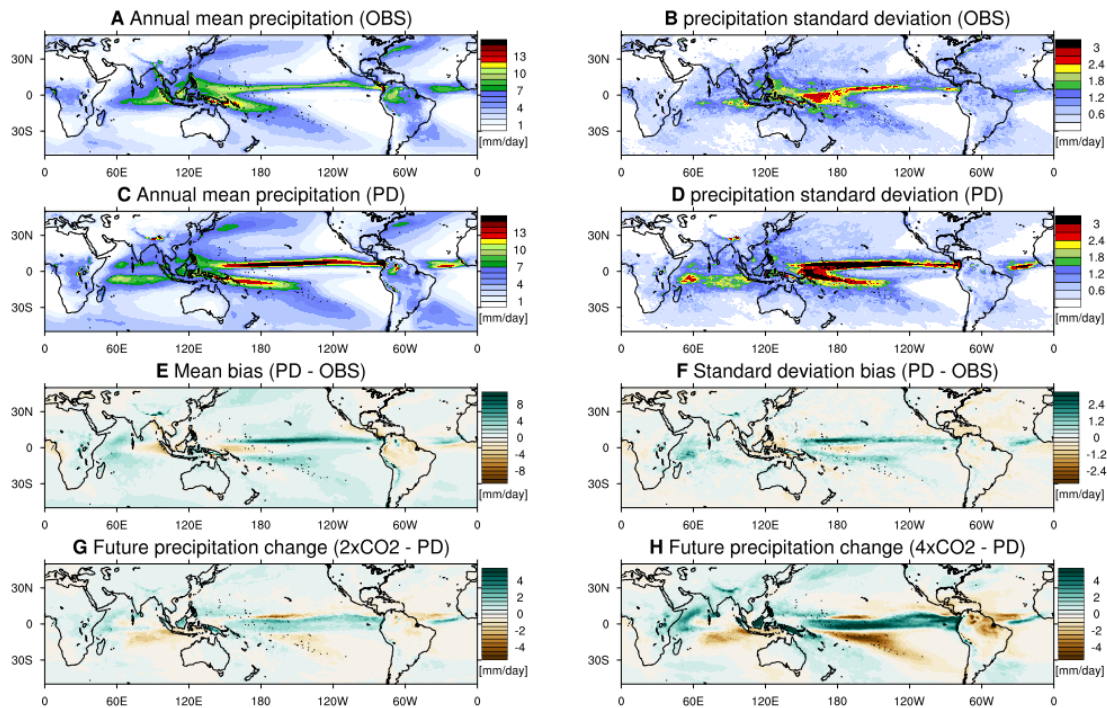


Figure S3. Same as in Figure S2 but for precipitation (mm day^{-1}). Observational data is from the Tropical Rainfall Measurement Mission (TRMM)(24) 3B43 product during the 1999-2018 period.

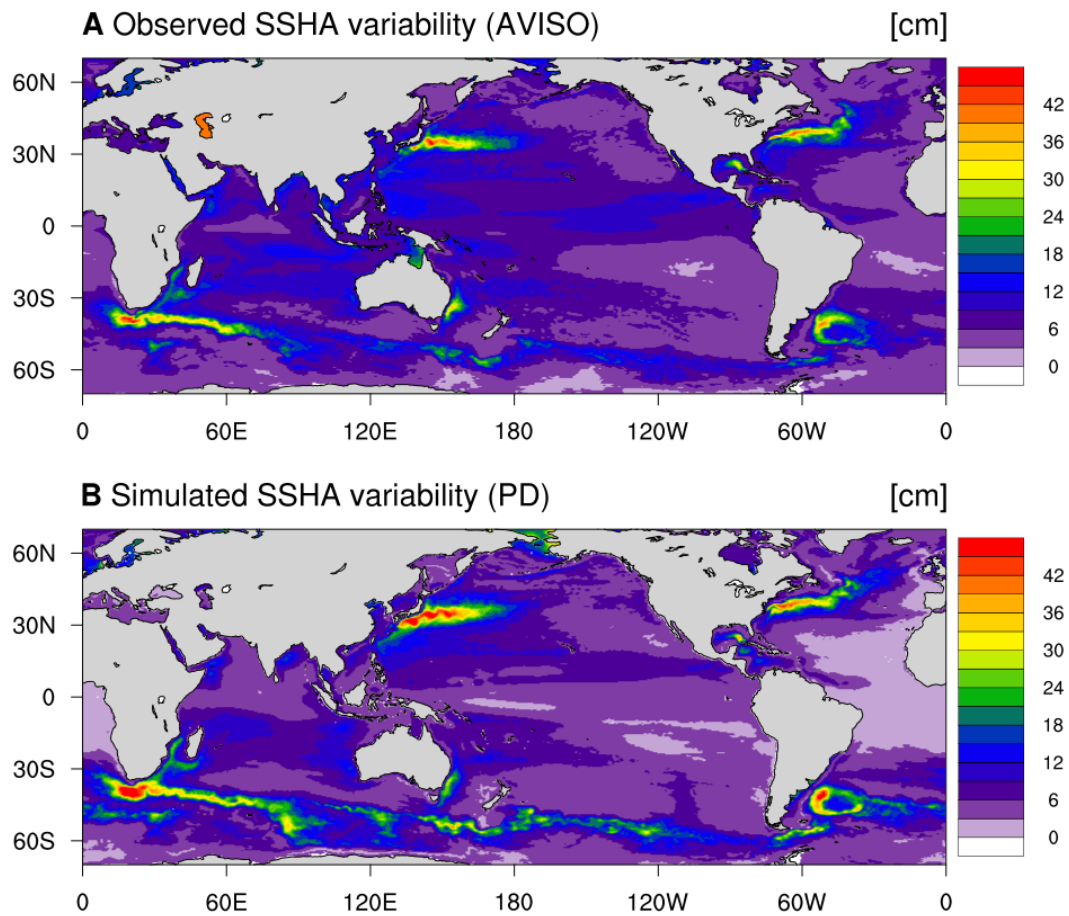


Figure S4. Standard deviation of the daily sea surface height anomaly (SSHA) from (A) observation and (B) PD simulation. Observational data is obtained from Archiving, Validation and Interpretation of Satellite Oceanographic Data (AVISO)(51) merged product during the 1993-2018 period.

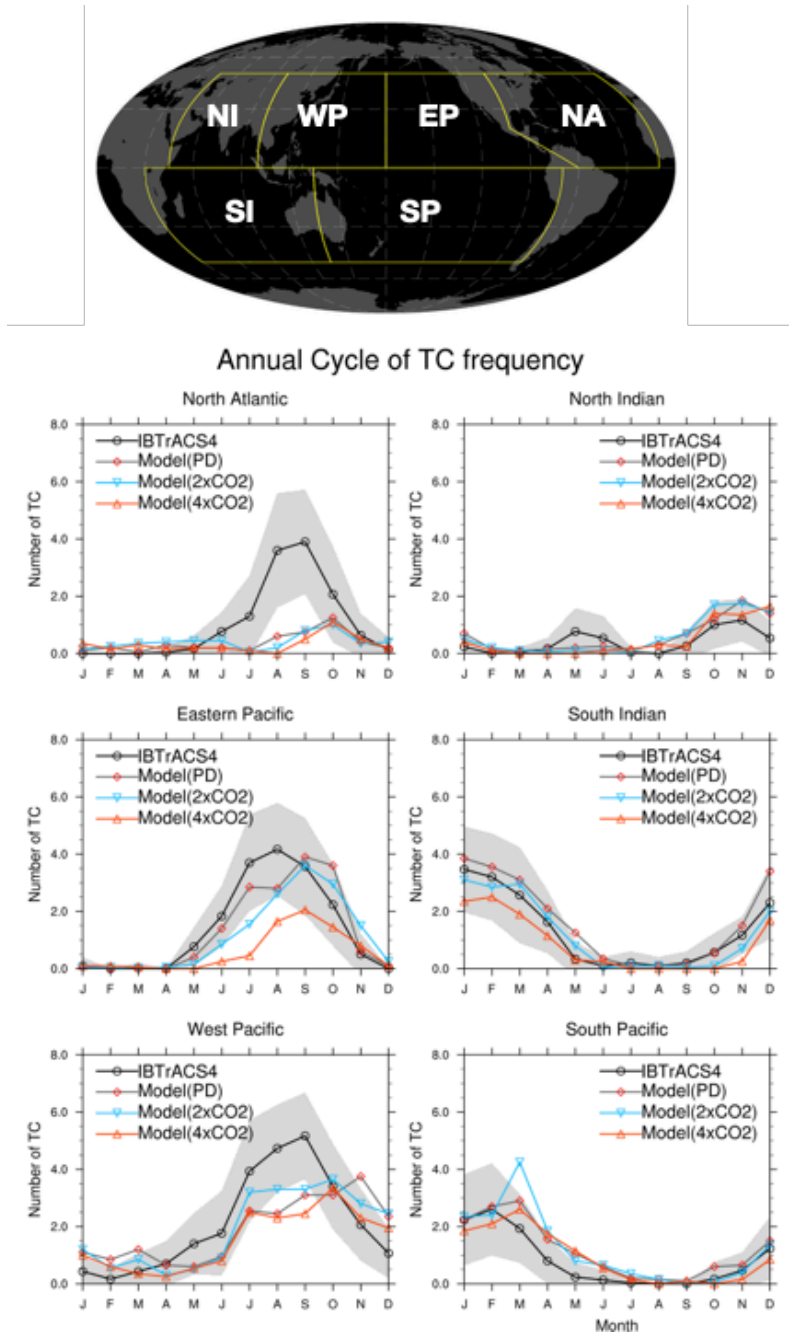


Figure S5. The domain of each basin (upper) and the annual cycle of monthly TC frequency (year^{-1}) from observations (black), PD (gray), $2\times\text{CO}_2$ (blue), and $4\times\text{CO}_2$ (red) simulations. Gray shadings show the range of year-to-year variability of TC frequency at each month.

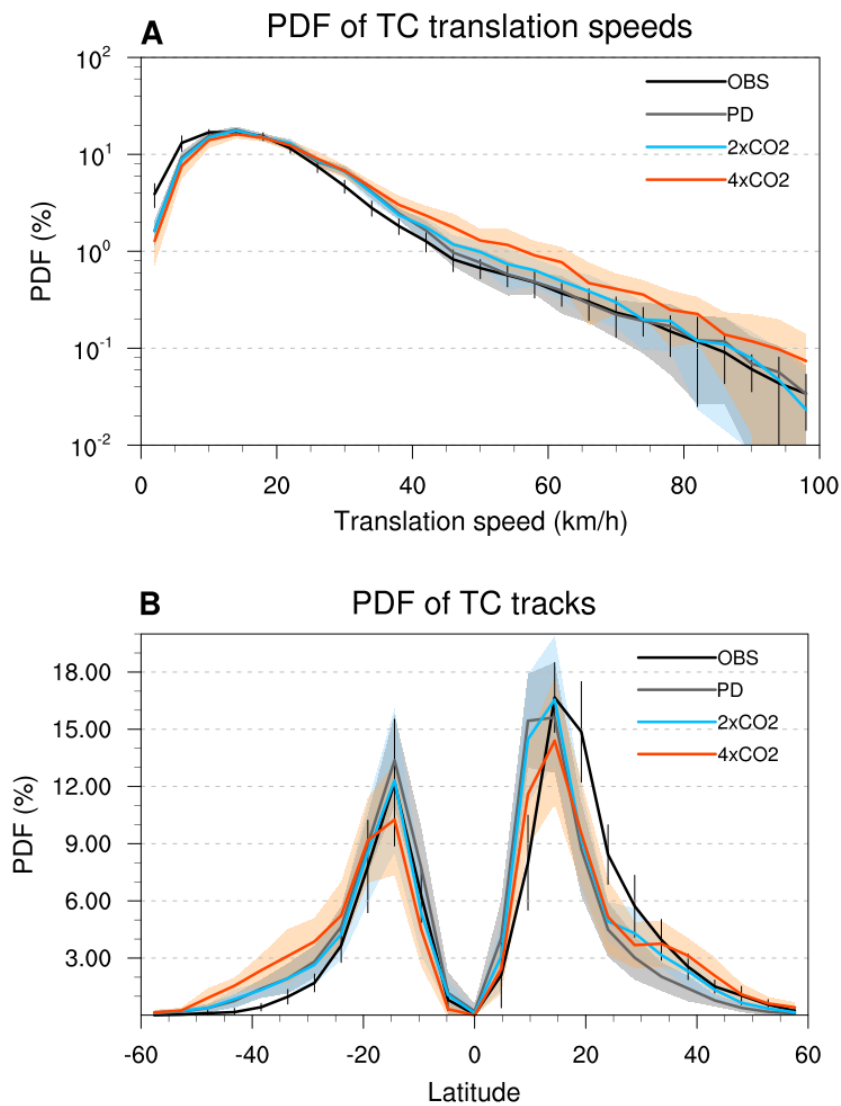


Figure S6. Probability density distributions of TC translation speeds and track latitude. (A) TC translation speeds and (B) track latitude in observations (black), PD (gray), 2×CO₂ (blue), and 4×CO₂ (red) experiments. Vertical bars indicate one standard deviation of interannual variability in the observation and shadings indicate one standard deviation of interannual variability for the simulations.

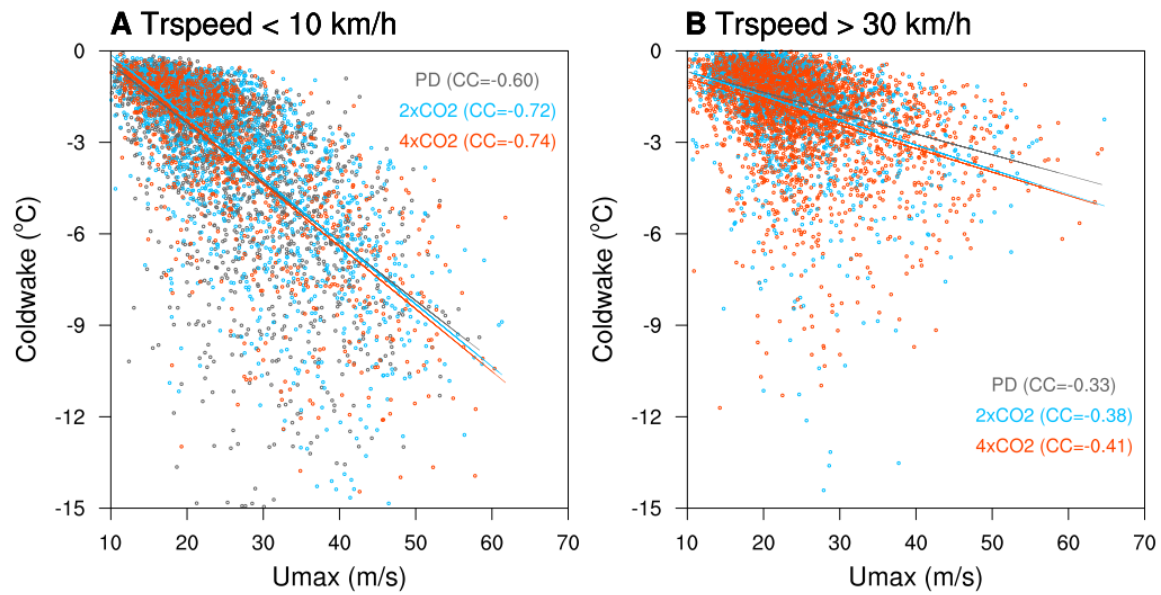


Figure S7. Relationship between cold wakes and maximum wind speed of TCs. The magnitude of cold wakes as a function of wind speed for (A) slow-moving TCs with translation speed of less than 10 km h^{-1} and (B) fast-moving TCs with translation speed of greater than 30 km h^{-1} in the PD (gray), $2\times\text{CO}_2$ (blue), and $4\times\text{CO}_2$ (red) experiments.

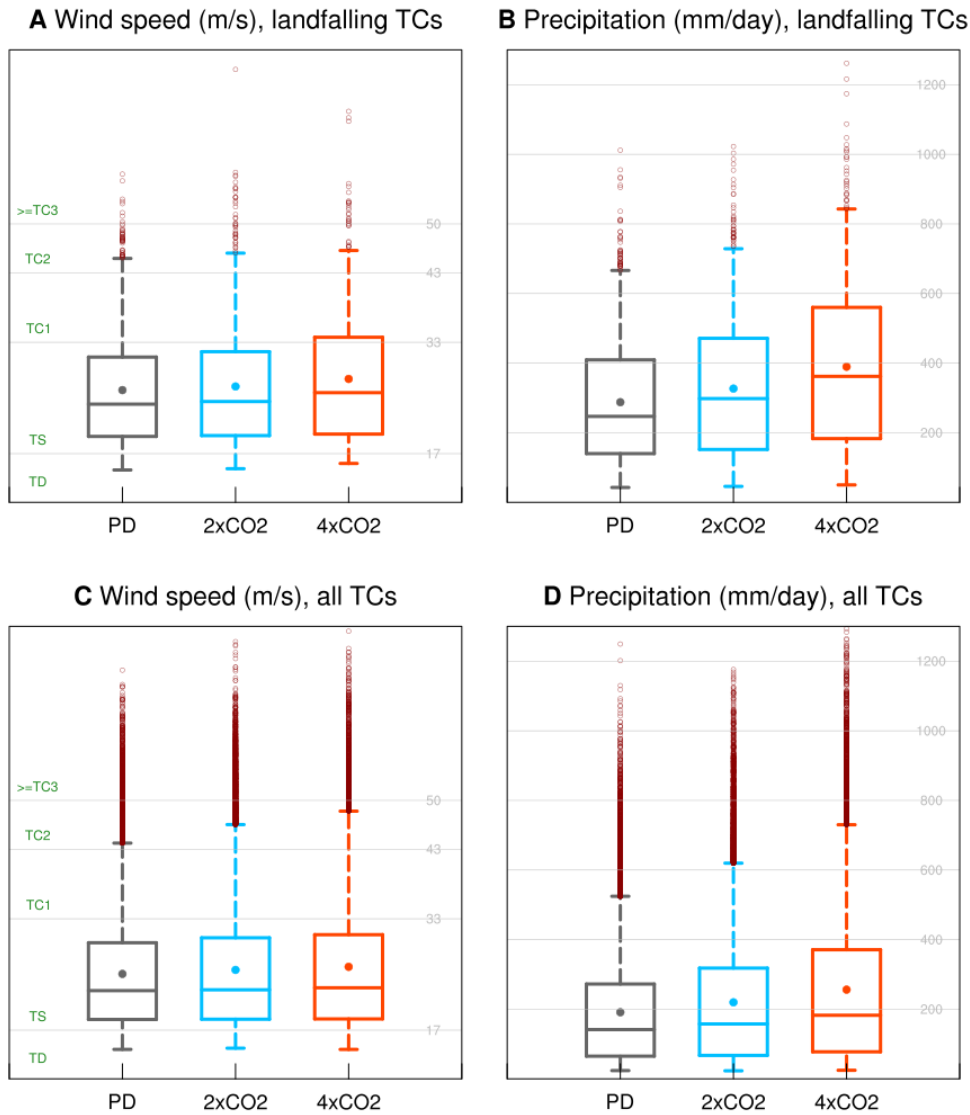


Figure S8. Box plots of (A and C) maximum wind speed (m s^{-1}) and (B and D) precipitation (mm day^{-1}) for (A and B) landfalling TCs and (C and D) all TCs in the PD (gray), $2\times\text{CO}_2$ (blue), and $4\times\text{CO}_2$ (red) experiments. The limits of whiskers represent the 5th and 95th percentiles. The limits of boxes represent the 25th and 75th percentiles. The line and circle inside the boxes indicate median and mean, respectively. Values above 95th percentiles line are marked as the open circles. To remove the impact of extratropical storms, TCs within 30°S to 30°N are considered.

Table S1. TC-related statistics for (A) observations, as well as the (B) PD, (C) 2×CO₂, and (D) 4×CO₂ experiments. Shown are the annual number of TCs, mean duration (days), mean travel distance (km), mean translation speed (km h⁻¹), and mean maximum wind speed (m s⁻¹). Values on the right of plus-minus sign (±) indicate the year-to-year standard deviation.

	(A) OBS (IBTrACS4)	(B) PD	(C) 2×CO ₂	(D) 4×CO ₂
nTC per year (≥TS)	85±9	85±11	79±9	58±6
mean duration (days)	9.0±0.9	6.9±0.5	6.5±0.5	5.9±0.5
mean travel distance (km)	3882±429	3196±252	3087±313	3005±328
mean translation speed (km h ⁻¹)	18.0±0.7	19.3±0.8	19.7±0.9	21.4±1.3
mean (U _{max}) (m s ⁻¹)	39.3±1.7	32.9±1.0	33.6±1.2	34.7±1.6

Table S2. List of observed cold wakes, including name of the TC, maximum SST cooling, latitude of the maximum cooling, and references.

Number	TC Name (year)	Maximum cooling (°C)	Latitude	Reference
1	Soulik (2018)	8.1	32 °N	(36)
2	Lupit (2010)	3.8	20 °N	(37)
3	Fanapi (2010)	2.5	24 °N	(37)
4	Malakas (2010)	3.0	24 °N	(37)
5	Megi (2010)	7.0	19 °N	(37)
6	Frances (2010)	2.1	22 °N	(37)
7	Ma-on (2011)	4.3	24 °N	(38)
8	Muifa (2011)	3.5	22 °N	(38)
9	Talas (2011)	1.1	24 °N	(38)
10	Kulap (2011)	1.0	20 °N	(38)
11	Roke (2011)	0.8	22 °N	(38)
12	Bolaven (2012)	2.0	20 °N	(38)
13	Sanba (2012)	0.8	24 °N	(38)
14	Prapiroon (2012)	3.3	22 °N	(38)
15	Kai-Tak (2000)	10.8	20 °N	(16)

References

- 1 Hurrell, J. W., Hack, J. J., Shea, D., Caron, J. M. & Rosinski, J. A New Sea Surface Temperature and Sea Ice Boundary Dataset for the Community Atmosphere Model. *Journal of Climate* **21**, 5145-5153, doi:10.1175/2008jcli2292.1 (2008).
- 2 Huffman, G. J. *et al.* The TRMM Multisatellite Precipitation Analysis (TMPA): Quasi-Global, Multiyear, Combined-Sensor Precipitation Estimates at Fine Scales. *Journal of Hydrometeorology* **8**, 38-55, doi:10.1175/jhm560.1 (2007).
- 3 Ducet, N., Le Traon, P. Y. & Reverdin, G. Global high-resolution mapping of ocean circulation from TOPEX/Poseidon and ERS-1 and -2. *Journal of Geophysical Research: Oceans* **105**, 19477-19498, doi:10.1029/2000jc900063 (2000).
- 4 Park, J.-H. *et al.* Rapid Decay of Slowly Moving Typhoon Soulik (2018) due to Interactions With the Strongly Stratified Northern East China Sea. *Geophysical Research Letters* **46**, 14595-14603, doi:10.1029/2019gl086274 (2019).
- 5 D'Asaro, E. A. *et al.* Impact of Typhoons on the Ocean in the Pacific. *Bulletin of the American Meteorological Society* **95**, 1405-1418, doi:10.1175/bams-d-12-00104.1 (2014).
- 6 Wada, A., Uehara, T. & Ishizaki, S. Typhoon-induced sea surface cooling during the 2011 and 2012 typhoon seasons: observational evidence and numerical investigations of the sea surface cooling effect using typhoon simulations. *Progress in Earth and Planetary Science* **1**, 11, doi:10.1186/2197-4284-1-11 (2014).
- 7 Chiang, T.-L., Wu, C.-R. & Oey, L.-Y. Typhoon Kai-Tak: An Ocean's Perfect Storm. *Journal of Physical Oceanography* **41**, 221-233, doi:10.1175/2010jpo4518.1 (2011).